

New-particle formation, growth and climate-relevant particle production in Egbert, Canada: Analysis from one year of size-distribution observations

5 **J. R. Pierce^{1,2}, D. M. Westervelt³, S. A. Atwood¹, E. A. Barnes¹, W. R. Leaitch⁴**

[1]{Department of Atmospheric Science, Colorado State University, Fort Collins, CO, USA}

[2]{Department of Physics and Atmospheric Science, Dalhousie University, Halifax, NS, Canada}

[3]{Program in Science, Technology, and Environmental Policy (STEP), Princeton University, Princeton, NJ, USA}

10 [4]{Environment Canada, Toronto, Ontario, Canada}

Correspondence to: J. R. Pierce (jeffrey.pierce@colostate.edu)

15 **Abstract**

Aerosol particle nucleation, or new-particle formation, is the dominant contributor to particle number in the atmosphere. However, these particles must grow through condensation of low-volatility vapors without coagulating with the larger, pre-existing particles in order to reach climate-relevant sizes (diameters larger than 50-100 nm), where the particles may affect clouds and radiation. In this paper, we use one year of size-distribution measurements from Egbert, Ontario, Canada to calculate the frequency of regional-scale new-particle formation events, new-particle formation rates, growth rates and the fraction of new particles that survive to reach climate-relevant sizes. Regional-scale new-particle formation events occur on 14-31% of the days (depending on the stringency of the classification criteria), with event frequency peaking in the spring and fall. New-particle formation rates and growth rates are similar to those measured at other mid-latitude continental sites. We calculate that roughly half of the climate-relevant particles (with diameters larger than 50-100 nm) at Egbert are formed through new-particle formation events. With the addition of meteorological and SO₂ measurements, we find that new-particle formation at Egbert often occurs under synoptic conditions associated with high surface pressure and large-scale subsidence that cause sunny conditions and clean-air flow from the north and west. However, new-particle formation also occurs when air flows from the polluted regions to the south and southwest of Egbert. The new-particle formation rates tend to be faster during events under the polluted south/southwest flow conditions.

1. Introduction

35 Atmospheric aerosols may impact climate directly by scattering and absorbing solar radiation, and indirectly by modifying the albedo and lifetime of clouds (Forster et al., 2007). For both of these effects, aerosol particles with diameters larger than 50-100 nm dominate the climate effects since (1) accumulation-mode (~100-1000 nm particles) tend to dominate the direct scattering/absorption effects in most parts of the atmosphere (Charlson et al., 1992; Seinfeld and Pandis, 2006) and (2) particles larger than about 50-100 nm act as Cloud Condensation Nuclei (CCN), the seeds upon which cloud
40 droplets form (e.g. Dusek et al. (2006); Seinfeld and Pandis (2006)). The actual lower cutoff diameter for CCN depends on the updraft velocity in the cloud and the composition of the aerosols.

Aerosol nucleation, the formation of new ~1-nm particles by the aggregation of low-volatility vapor molecules (including sulfuric acid, organics, ammonia and water), is likely the largest contributor to aerosol number in the atmosphere (Kulmala et al., 2004; Pierce and Adams, 2009; Spracklen et al.,
45 2006). When nucleated particles grow to sizes where they are measured in the atmosphere (between 1-10 nm depending on the measurement instruments), the phenomena is generally called new-particle formation to distinguish these measured events from nucleation, which is generally not measured directly. New-particle formation has been observed in a large number of continental boundary-layer (BL) locations, the free troposphere and some marine locations (e.g. Kulmala et al. (2004) and
50 references therein).

While new-particle formation occurs in many regions of the atmosphere and contributes a significant number of particles, these new particles must grow to larger sizes (50-100 nm) in order to have an appreciable effect on climate. The growth of the new particles occurs primarily through the condensation of sulfuric acid vapor and low-volatility organic vapors (Boy et al., 2005; Kuang et al.,
55 2012; Kulmala et al., 2005; Riipinen et al., 2011, 2012). However, these growing particles may be removed, primarily by coagulation with larger particles, before reaching climate-relevant sizes. The competition between condensational growth and coagulation losses has led to the adoption of the term Survival Probability (SP) for the fraction of newly formed particles that grows to a climate-relevant size without being scavenged through coagulation (Kuang et al., 2009; Pierce and
60 Adams, 2007; Westervelt et al., 2013). In environments with a large source of condensable vapors and a low amount of pre-existing particles, new particles grow quickly (both due to the high production of condensable vapors and the low sink of condensable vapors to the pre-existing particles) and are lost by coagulation slowly. Under these conditions, the survival probability is high and has been observed to

65 exceed 99% (to 50 nm) in some atmospheric conditions (Westervelt et al., 2013). On the other hand, under conditions with a small source of condensable vapors and a high amount of pre-existing particles, the survival probability is low and has been observed to be less than 1% under these conditions (Westervelt et al., 2013). In order to understand how new-particle formation contributes to climate-relevant aerosol concentrations, both new-particle formation rates and survival probabilities must be understood in different atmospheric regions and under varying conditions.

70 New-particle formation may occur over relatively small spatial scales (kilometers or smaller) in plumes from individual sources or clumps of sources (e.g. an urban plume) (Junkermann et al., 2011; Lonsdale et al., 2012; Stevens and Pierce, 2013; Stevens et al., 2012; Yu, 2010), or it may occur more homogeneously over relatively large spatial scales (100s of kilometers) when a synoptic air mass is relatively homogeneous for both aerosols/gases and meteorology (Jeong et al., 2010). For
75 regional-scale new-particle formation, formation and growth rates may be calculated from the timeseries of aerosol size-distribution measurements at stationary sites (Dal Maso et al., 2005). This is done by observing how the number of particles at the smallest sizes changes with time and by tracking the growth in the diameter of these particles. These properties can be calculated only when the air mass is relatively homogeneous. In air masses that have aerosol size distributions that vary spatially, aerosol
80 size distributions will change due to advection. If the air mass is assumed to be homogeneous in cases where it is not, there may be apparent appearances, disappearances, growth or shrinking of particles that are not due to physical new-particle formation and growth. In these inhomogeneous cases, particles formed via new-particle formation are still observed by stationary measurement sites, but the air-mass properties change too quickly to determine the formation and growth rates.

85 Recent studies have used observations of regional new-particle formation and growth to determine the survival probability of particles at various measurement sites (Kuang et al., 2009; Westervelt et al., 2013). These studies show that if the air mass over a measurement site is homogeneous for long enough, the growth of new particles to climate-relevant sizes may be explicitly tracked. These direct observations of new-particle formation rates, growth rates and new-particle
90 survival probability are essential for testing the ability of aerosol microphysics models to correctly predict the sources of CCN and other climate-relevant particles in the atmosphere. Westervelt et al. (2013) used the observed values from five locations to test multiple nucleation schemes in the GEOS-Chem-TOMAS global chemical transport model with online aerosol microphysics, and the model generally reproduces new-particle formation and growth frequency and rates at these locations.

95 Additionally, Kerminen et al. (2012) calculated the contribution of new-particle formation to CCN concentrations at four locations by looking at the change in CCN concentrations before and after the growing nucleation mode reached a CCN size threshold. Thus, they were able to calculate the CCN contribution without using growth rates and survival probabilities.

100 Given that these recent studies have quantified the contribution of regional new-particle formation events to the production of climate-relevant particles in several locations, it is useful to understand the factors that contribute to the occurrence of regional new-particle formation events in order to further test model predictions. Previous studies demonstrate that more intense solar radiation (which enhances photochemistry), high concentrations of precursor species of low-volatility condensable material (e.g. SO₂ and biogenic volatile organic compounds), and low concentrations of pre-existing aerosols (i.e. a low condensation and coagulation sink) all create favorable conditions for regional new-particle formation and growth (Donahue et al., 2011; Kulmala et al., 2005; Pierce et al., 2011, 2012; Sihto et al., 2006). Thus, measurement sites that can provide statistics on new-particle formation rates, growth rates, survival probabilities along with information on the factors that contribute to new-particle-formation/growth events will provide a basis for testing fundamental physical and chemical processes in aerosol models.

115 In this study, we use one year of size-distribution measurements (May 2007 – May 2008) to determine statistics on regional new-particle formation, growth and survival probability to climate-relevant sizes at Egbert, Ontario, Canada. Additionally, we look at the environmental factors that control the occurrence of these events at this location. Egbert generally experiences remote continental air when air masses move from the north and generally more polluted when air masses move from the south (Rupakheti et al., 2005); thus, like many mid-latitude continental locations, Egbert experiences a mixture of natural and anthropogenic influences (Slowik et al., 2010). New-particle formation at Egbert was explored for a 3-week period with 4 other Ontario sites (Jeong et al., 2010), and new-particle formation at Egbert for a full year was investigated for coherence with new-particle formation with a site in Indiana, US (Crippa and Pryor, 2013), but neither of these studies presented comprehensive statistics on new-particle formation, growth and the contribution to climate-relevant particles.

120 In the following section, we describe the methods for our analysis. In section 3, we present our results, including the statistics of new-particle formation, growth and survival probability at Egbert as

125 well as an analysis of the meteorological and chemical factors associated with the new-particle
formation and growth events. The conclusions are in section 4.

2. Methods

2.1. Location

The measurements in this paper were taken from 3 May 2007 until 15 May 2008 at the Center for
130 Atmospheric Research Experiments (CARE) in Egbert, Ontario, Canada (44.23 °N, 79.78 °W; 251 m
a.s.l) operated by Environment Canada. Egbert is located ~70 miles north of Toronto. While the
region close to Egbert is a mixture of forests and farmland, Toronto and the southern Ontario region has
~8 million people. Thus, when winds are from the south, Egbert is influenced by the outflow from the
densely populated southern Ontario region as well as the US northeast. When winds are from the
135 north, the air generally has little recent anthropogenic influence (an exception is industry in the isolated
city of Sudbury ~300 km to the north) and may have significant biogenic influence during the spring,
summer and early fall (Slowik et al., 2010).

2.2. Instrumentation

The base meteorological measurements at the Egbert site include pressure, temperature, relative
140 humidity, wind speed and direction (using a R.M. Young Model 05103 Wind Monitor) and solar
irradiance. During 2007 to 2008, the ambient aerosol number size distribution was measured with a
Scanning Mobility Particle Sizer (SMPS) system comprised of a TSI 3071 Electrostatic Classifier and a
TSI 3010 Condensation Particle Counter (UCPC), which measured the size distribution from 10– 420
nm with a time resolution of about 5 minutes. Flows were calibrated with Gilibrator and sizing was
145 checked several times during the year with nearly monodisperse particles generated from a separate
Electrostatic Classifier as well as with particles of polystyrene latex. Additional details of the SMPS
system are discussed in Riipinen et al. (2011). SO₂ measurements were made with a TECO 43-S Sulfur
Dioxide Monitor. Calibrations were done using a NIST traceable SO₂ gas source and a dilution system.
The detection limit was 200 pptv for the 15-minute averages that we use here.

150 **2.3. New-particle formation, growth and survival probability analysis**

2.3.1 Event classification

We classify new-particle formation events each day using the event classification routine of Dal Maso et al. (2005), and a brief description of this classification follows. A total number of 327 days are analyzed, which is fewer than the total number of days (370) because we exclude days that do not have SMPS measurements for at least 75% of the day's duration (the sample time resolution is ~5 minutes). We classify each day as either a new-particle-formation event day or a non-event day. To be considered a new-particle-formation event day a distinct mode of particles with diameters smaller than 20 nm must appear during the day (regardless of the time at which it appears). This classification (and the event classification described below) is done visually and subjectively as in Dal Maso et al. (2005).

160 For days that are considered new-particle formation days, we classify events as class I, class II and undefined event days, also following Dal Maso et al. (2005) with the exception that our class 2 events encompass both the class 2 events and the “undefined” events in Dal Maso et al. (2005) as there was a strong continuum between these two event types in the Egbert data (most of the focus of this paper will be on the class 1a and 1b events that may be regional events). However, we do not sub-classify I events to Ia and Ib events as in Dal Maso et al. (2005) as the nucleation mode is generally always distinguishable from the background distribution (Ia events in Dal Maso et al. (2005)). Examples of each class are given in Figure 1; however, even within event classes, there is significant variability between event days in terms of observed behavior.

170 Class I days (e.g. Figure 1a) exhibit new-particle formation and an obvious, traceable growth of the nucleation mode to at least 50 nm before the nucleation mode disappears. Class I days are most likely widespread, regional new-particle formation events with a relatively homogeneous air mass advecting over the Egbert measurement site. The example in Figure I shows an air mass that is not completely homogeneous as the growth in the nucleation mode is not smooth. However, we are still able to retrieve formation and growth rates on these days.

175 Class II days (e.g. Figure 1b) exhibit new-particle formation and some growth (in some cases to over 50 nm); however, we do not trust the new-particle formation, growth and survival probability statistics on class II days to the same degree as class I events due to a variety of factors. These factors include possible changes in the air mass during the growth, shrinking after the growth (which may be a sign of a plume event), or it not being clear if the growing particles are the same particles as the newly

180 formed particles (as is the case in Figure 1b). Class II events may be regional in nature, but the air mass is not homogeneous enough to clearly track new-particle formation and growth from the stationary Egbert site.

Undefined events (e.g. Figure 2) exhibit particles measured at the smallest sizes of the SMPS, and there is either no growth or there is growth followed by shrinking (as is the case in Figure 1c).
185 These events may be particles that nucleate across spatial scales smaller than regional-scale events, such as point-source or urban plumes, or they may be regional events in a relatively inhomogeneous or changing airmass. They may also be small primary particles from nearby sources. Cases where particles appear to grow and then shrink may indicate plume nucleation events where the direction of the wind changes with time: The smallest particles are observed when the edges of the plume are over
190 the measurement site, and the larger new particles are observed when the center of the plume is over the measurement site. Larger new particles (particles that nucleate closer to the source and have more time to grow) are observed in the middle of plumes with more-recently nucleated particles towards the edges (Stevens et al., 2012).

2.3.2 New-particle formation and growth rates

195 The details of the calculation of new-particle formation and growth rates are discussed in detail in Westervelt et al. (2013) and Kulmala et al. (2012), but we briefly summarize them here. The rate of new-10nm-particle formation (J_{10}) is calculated from the time-dependent change in the nucleation-mode (defined here as 10-25 nm) concentrations from the SMPS. We correct these formation rates for the coagulation loss rate of these particles and the loss of particles by
200 condensational growth to sizes larger than 25 nm. The correction for these coagulation and condensational losses increases the calculated J_{10} from the uncorrected values. We implicitly assume that all particles entering the 10-25 nm size range are from new-particle formation during class I and II events and not from primary emissions. In this paper, we present J_{10} values as both the mean J_{10}
205 during the period where new-particle formation is occurring as well as 24-hour mean values to normalize the total particle production between short and long events.

The particle diameter growth rates (GR) are calculated by tracking the change in the diameter of the peak value of the aerosol size distribution for the growing nucleation mode between 10 and 25 nm. We use a linear fit of the peak diameter (defined by maximum concentration) over time to estimate the mean growth rate during the observable growth period. When able, we also calculate the mean growth

210 rate between 25 and 50 nm and between 25 and 100 nm using the same technique. Each of these
growth rates is used for calculating the survival probability to 50 and 100 nm (described next).
Growth-rate statistics are presented for the 10-25 nm size range.

2.3.3 Survival probability and climate-relevant particle formation rates

We calculate the survival probabilities to 50 and 100 nm (SP50 and SP100, respectively) by using the
215 Probability of Ultrafine Growth (PUG) model (Pierce and Adams, 2007). These 50 and 100 nm cutoffs
are used as proxies for CCN cutoffs; however, CCN cutoffs also vary as a result of aerosol composition
(e.g. Paramonov et al., (2013)). The application of the PUG model to SMPS measurements is
described in detail in Westervelt et al. (2013). The PUG model calculates the SPs using the mean GRs
described above and the coagulation sink of the growing particles to larger, pre-existing particles. The
220 coagulation sink represents the first-order loss rate of the growing particles by coagulation, and we
calculate it using the measured SMPS size distributions and Brownian coagulation theory (Seinfeld and
Pandis, 2006). The PUG model calculates the survival probability over small, incremental steps of
growth (~2 nm for 10-nm particles and ~10 nm for 100 nm particles; these are the bin spacings of the
SMPS) by calculating how many particles will be lost by coagulation in the time it takes the particles to
225 grow by the incremental amount. For each growth step, the coagulation sink is recalculated. The
overall survival probabilities to 50 or 100 nm are calculated as the products of the probabilities of
surviving each incremental step.

We calculate the formation rates of climate-relevant particles (J50 and J100) as the product of
the J10 with SP50 (for J50) and J10 with SP100 (for J100). We present J50 and J100 as 24-hour-mean
230 values rather than the event-mean values to represent the mean climate-relevant particle production
rates on event days. These values are used to estimate the total contribution of regional-scale
new-particle formation events to 50 and 100 nm particle concentrations.

2.4. Reanalysis meteorology and back trajectories

We use the NCEP/NCAR Reanalysis (Kalnay et al., 1996) to investigate the large-scale meteorology on
235 event days. Specifically, we analyze the fields of 500 hPa geopotential heights, surface pressures and
large-scale vertical velocities (omega) at time-steps that are the closest to the time of the new-particle
formation events.

In order to assess the meteorological conditions and source regions associated with air masses

arriving at Egbert, we utilize back trajectory analysis. The NOAA HYSPLIT Lagrangian trajectory
240 model (Draxler, 1999; Draxler and Hess, 1997, 1998) is run using the GDAS 1°x1° meteorological
dataset supplied by the NOAA Air Resources Laboratory. Back trajectories are shown for 24-hours
prior to their arrival at 100 m above ground level at Egbert. We generate eight trajectories per day with
the trajectory arriving closest to the period of interest (e.g. the middle of a new-particle formation
event) selected as characteristic of surface level transport at that time. Note that we also examined other
245 arrival heights, but these were found to be similar to the 100 m heights for trajectories arriving within
the boundary layer (0 m, 500 m) and not characteristic of transport to the surface for arrival heights
above the typical boundary layer (1500 m).

3. Results

Figure 2 shows the fraction of days in each month that exhibited class I, II, undefined events and
250 non-events. Each month provides at least 22 days with sufficient SMPS data for this analysis (10
months had at least 26). The potentially regional new-particle formation classes, I (observable and
quantifiable growth of new particles) and II (similar to I but less confidence in quantification), exhibit
bimodal seasonal cycle with peaks in the spring and the fall. Either class I or II events occur on about
half of the days during the peak seasons and only about 20% of the days during summer and winter
255 (except January where there was only one II event and no I events). Most of the class I+II seasonality
is driven by the seasonality of the class I events. The winter minimum in class I and II event frequency
may be due to a low source of biological volatile organic compounds (BVOCs), precursors for
secondary organic aerosols that may be involved in new-particle formation and growth (Riipinen et al.,
2011, 2012) as well as lower solar radiation, during cold months. Unfortunately, we do not have
260 measurements of BVOCs or aerosol organics throughout this full time period. The summer minimum
may be due to the minimum monthly mean SO₂ mixing ratios occurring during July and August.
Monthly mean SO₂ mixing ratios are 0.6-0.7 ppbv during these summer months and 1-2 ppbv during
the other months. Additionally, a proxy we use for H₂SO₄ concentrations (described in section 3.2) also
has a minimum during the summer. We go into more detail regarding these factors and the occurrence
265 of new-particle formation events in section 3.2.

Undefined events (no quantifiable growth after new-particle detection), which may be
plume-scale formation events or plumes of ultrafine primary emissions, tend to be most frequent during
the winter. Up to 80% of the days during the winter and ~35% of days during the summer are

undefined days. As some undefined events occur on days where class I and II events also occur (but these events are ignored here), this may be an upper bound of the season cycle because there may be undefined events hidden in class I and II event days. Note, for days where undefined events occur on class I and II days, we do not include the contribution of the undefined events to the class I and II statistics. Regardless, non-event days peak during the summer (nearly 40% of days during July), which may be related to the low SO₂ mixing ratios and H₂SO₄ proxy during the summer as mentioned earlier.

275 **3.1. Particle formation rates, growth rates and CCN formation**

Figure 3 shows cumulative distribution functions for J10, GR, SP50, SP100, J50 and J100 for the full year of measurements. The medians and means for these distributions as well as the total number of days in each event class are shown in Table 1. J10 and GR statistics are presented for class I days as well as the sum of class I and II days (we have less confidence in these values due to the inclusion of class II days). We present survival probability, J50 and J100 statistics only for class I days as most class II days do not exhibit growth to at least 50 nm. For J10, we present both the new-particle formation rate averaged over the period where new-particle formation was observed (usually 2-4 hours) as well as the 24-hour average rate over the day (which leads to values generally 5-10x lower than the values during the event period). J50 and J100 values are the 24-hour average values. The 24-hour average values are useful in that the total daily and annual production rates may be calculated from these values without needing to know the duration of each event.

The event-mean J10 values on class I days range from under 0.1 cm⁻³ s⁻¹ to about 10 cm⁻³ s⁻¹ with a mean of 0.84 cm⁻³ s⁻¹ and median of 0.64 cm⁻³ s⁻¹. These values are about 25-50% lower when class II days are also included due to class II days having somewhat lower particle formation rates in general. As stated above, the 24h mean J10 values are 5-10x lower than the event-mean values. For class I days, the annual mean and median values of the 24-h mean formation rates are 0.13 and 0.12 cm⁻³ s⁻¹, respectively. The mean, median and data range are consistent with the range of values given for non-urban continental sites in the review paper by Kulmala et al. (2004). Westervelt et al. (2013) presented 24-hour-mean new-particle formation rate statistics at 3 nm (J3) for 5 locations (Pittsburgh, Hyytiälä, Atlanta, St. Louis and the Po Valley) and find that the observed annual means for the 24-hour J3s at these locations range from 0.58 to 8.7 cm⁻³ s⁻¹, and the annual medians range from 0.09 to 0.55 cm⁻³ s⁻¹. These J3 values are generally larger than the J10 values derived here for Egbert; however, J10 values include the loss of particles by coagulation as the particles grow between 3 and 10 nm, which

cause J10 values to be lower than J3. We estimate the mean survival probability between 3 nm and 10
300 nm to be 25% for the Egbert study, which gives us estimated mean/median J3s of about $0.5 \text{ cm}^{-3} \text{ s}^{-1}$, in
line with the estimates of Westervelt et al. (2013).

Diameter GRs range from less than 0.5 to about 10 nm hr^{-1} and are similar on class I and II
days. The mean GR is 3.1 nm hr^{-1} and the median is 2.2 nm hr^{-1} . Again, these mean, median and range
of values are consistent with range of values presented for non-urban continental sites in Kulmala et al.
305 (2004). These mean and median values are at the low end of the range in Westervelt et al. (2013) at the
5 locations. At these locations, GR means range from 2.8 to 6.9 nm hr^{-1} and medians range from 2.4 to
 5.8 nm hr^{-1} . The SP50 values at Egbert range from 1% to close to 100% depending on the event, and
the SP100 values at Egbert range from 0.3% to over 90% with a mean and median of 19% and 7% (the
mean is higher than the median due to 2 high outliers, see Figure 3).

We calculate J50 as the product of J10 and SP50 for each class I event. The J50 values range
310 from 0.001 to about $0.2 \text{ cm}^{-3} \text{ s}^{-1}$, averaged over the full 24 hours of each class I day. The mean and
median values are 0.039 and $0.029 \text{ cm}^{-3} \text{ s}^{-1}$, respectively, and lie within the range found at the 5 sites in
Westervelt et al. (2013). Similarly, J100 is calculated as the product of J10 and SP100 for each class I
event. The J100 values range from 0.001 to about $0.2 \text{ cm}^{-3} \text{ s}^{-1}$, averaged over the full 24 hours of each
315 I-event day. The mean and median values are 0.022 and $0.009 \text{ cm}^{-3} \text{ s}^{-1}$, respectively. These values are
larger than 4 of the 5 sites in Westervelt et al. (2013) (the polluted Po Valley, Italy site is the exception)
due to the larger SP100 values at Egbert. The median formation rates correspond to about 2500 cm^{-3}
new N50 and 790 cm^{-3} new N100 on each event day. Compared to the four sites examined in
Kerminen et al. (2012), our Egbert climate-relevant particle formation amounts are similar to the
320 amounts at Botsalano, South Africa site but are larger than the rates at the three other sites, which are
located in northern Europe. However, Kerminen et al. (2012) use a different technique for calculating
the contribution of new-particle formation to climate-relevant sizes, which may lead to some
differences.

One can use the J50 and J100 values to estimate the contribution of regional new-particle
325 formation events to the number of climate-relevant particles in the region near Egbert. The formula
that we use is as follows.

$$\overline{N50}_{NPF} = \frac{\overline{J50} \cdot f_{1a} \cdot L50}{BL_{rise}} \quad (1)$$

Where $\overline{N50_{NPF}}$ is the annual-mean concentration of particles larger than 50 nm due to regional-scale NPF at Egbert, $\overline{J50}$ is the mean formation rate of 50-nm particles on class I event days ($0.039 \text{ cm}^{-3} \text{ s}^{-1}$), f_I is the fraction of analyzed days that are class I event day ($44/327=0.135$), $L50$ is the lifetime of particles larger than 50 nm in the boundary layer near Egbert, and BL_{rise} is the ratio of the boundary layer height when the nucleation mode reaches 50 nm to that when it reached 10 nm. Croft et al. (2013) show that the lifetime of CCN-sized particles in the boundary layer in the mid-latitudes is around 2-4 days, so we use a value of 3 days. Aircraft measurements of boundary-layer properties near Egbert show that the BLH increases from late morning (when the nucleation mode generally reaches 10 nm) to mid afternoon (when the nucleation mode generally reaches 50 nm) by about a factor of 2, so we set $BL_{rise} = 2$. With these assumptions, we calculate a $\overline{N50_{NPF}}$ of 700 cm^{-3} . The mean measured N50 throughout the entire time period was 1700 cm^{-3} . This means that about 40% of the N50 in the region around Egbert are formed from regional-scale boundary-layer new-particle-formation events.

335 However, there are uncertainties in $L50$ and BL_{rise} . Thus, the 40% contribution calculated here could easily be 20% or 60% within the range of uncertainties of these assumptions. Regardless, it is clear the new-particle formation contributes to a significant portion of the climate-relevant particles near Egbert.

We repeat the calculation to estimate $\overline{N100_{NPF}}$ from J100. If we assume that $L100$ is the same as $L50$ and that BL_{rise} is the same as the previous calculation, $\overline{N100_{NPF}}$ is 400 cm^{-3} . The mean measured N100 throughout the entire time period is 710 cm^{-3} . Our estimate of regional-scale boundary-layer new-particle formation to N100 is thus 56%. This estimate is larger than our predicted contribution of regional-scale boundary-layer new-particle formation to N50 (40%). Primary emissions tend to contribute to a larger fraction of the particles with increasing size, so this result is not physically consistent. There are three reasons why our $\overline{N100_{NPF}}$ calculation may be too high relative to our $\overline{N50_{NPF}}$ calculation: (1) The lifetime of 100-nm particles is likely shorter than 50-nm particles as 100-nm particles will act as CCN in a larger fraction of clouds, and thus 100-nm particles are more susceptible to wet deposition. (2) The boundary layer may grow in depth between the time the nucleation mode reaches 50 nm and when it reached 100 nm. (3) The 2 highest SP100 days shift the mean SP100 (19%) significantly above the median (7%). If we had a larger sample of event days, it is possible that the mean would be closer to the median, and the fractional contribution of new-particle formation to 100nm particles would be lower than the fractional contribution of new-particle formation to 50nm particles.

345
355

These estimated contributions of new-particle formation to CCN-sized particles (40-56%) are

similar to the global boundary-layer contribution of new-particle formation to CCN-sized particles
360 estimated in the modelling study by Merikanto et al. (2009); however, they show that much of this
contribution is due to new-particle formation in the free troposphere (with subsequent subsidence into
the boundary layer) rather than boundary-layer new-particle formation.

3.2. Conditions during new-particle formation events

Figure 4 shows box-whisker plots for the atmospheric conditions on each type of event and non-event
365 day. For event days, the values for each variable are taken as the mean value between the start and end
of new-particle formation (the period where new particles are arriving at diameters of ~10 nm). For
non-event days, the values for each variable are taken from the mean time of day for class I
new-particle formation events (approximately 11:00-16:00 local standard time) since there is no
new-particle-formation event time to draw upon. We display the statistical significance of differences
370 between the distributions of each event class using the Mann-Whitney U test. Although not shown on
the plots, the distributions for class I days are statistically different from non-event days to at least the
97% level for all factors except for temperature (81%) and condensation sink (76%).

Solar radiation drives photochemistry and thus the oxidation of SO₂ to form condensable H₂SO₄
and volatile organic compounds to form condensable organic species (Ehn et al., 2014). Previous
375 studies (e.g. Petäjä et al. (2009)) have shown that new-particle formation events are strongly correlated
with solar radiation. Solar radiation on class I and II days are significantly higher than undefined and
non-event days. All class I events occur between 7 AM and 7 PM local standard time, and all but 2
(out of 57) II events occur during this time window (not shown). On the other hand 15 (out of 164)
undefined events occur outside of this window (not shown) (the non-event solar radiation stats are
380 taken from ~11:00-16:00 the mean event time period for I events). These time-of-day differences
explain part of the differences in solar radiation; however, differences in large-scale meteorology (and
their effects on cloud cover) between event days are likely important too, as will be shown shortly.
Class I days have higher solar radiation than class II days, on average. Thus, similar to the previous
studies, the amount of solar radiation likely plays a role in initiating clearly defined regional-scale
385 new-particle formation events, and nighttime chemistry appears to be less important as I and II events
generally do not occur during dark hours.

While some nucleation theories (e.g. Vehkamäki et al. (2002)) predict increasing nucleation
rates with relative humidity, the data (as well as other observations, e.g. (Hamed et al., 2011)) show a

390 general anti-correlation between new-particle formation and relative humidity (relative humidity generally increases moving from class I to II to undefined to non-events). This increase in relative humidity is likely not causally linked to the likelihood of regional-scale new-particle formation events, but rather (1) clouds are more likely when the relative humidity is higher, (2) the relative humidity is generally higher at night, and (3) the condensation sink generally increases with relative humidity due to aerosol water uptake. While the difference in relative humidity between class I and II events with 395 undefined events and non-events is statistically significant, the difference between the I and II events is not.

Temperature anomalies (difference of the event-time temperature from the 4-week running mean) are mostly positive for class I days (75% of the events) and the data show a decreasing trend moving from class I to class II to undefined events; however, the difference between successive classes 400 are not significant to the 95% level. Although the difference between class I events undefined events is significant; however, some of these differences may be due to differences in event time of day. The cause of the higher mean/median temperature anomaly on class I days may be due to clear skies from large-scale meteorology and is consistent with the solar-radiation and relative humidity statistics (as will be discussed in the next subsection).

405 Surface pressure anomalies (also the difference of the event-time pressure from the 4-week running mean) are mostly positive for class I days (75% of the events) with decreasing values moving from class I to II to undefined to non-events. Differences between class I and class II events are not statistically significant, whereas the differences between these event classes with undefined and non-event days are statistically significant. The positive surface pressure anomaly for ~75% of the 410 class I and slightly less than 75% of the class II events shows that large-scale synoptic meteorology may have played a role in driving many of the regional-scale new-particle formation events. Surface highs in the mid-latitudes are associated with large-scale subsidence in the free troposphere, clear skies and lower-than-normal relative humidities. We will look regionally at differences in large-scale meteorology in the next subsection.

415 The condensation sink is the rate constant for condensation of a non-volatile condensable species from the vapor phase to the particle phase. Lower condensation sinks favor new-particle formation and growth because concentrations of condensable species may build up and lead to faster new-particle formation and growth rates. This has been observed in previous studies (e.g. Petäjä et al.

(2009); Sihto et al. (2006)). However, we find that class I event days have, on average, the highest
420 condensation sinks. The condensation sinks on class I days are higher than class II days (though only
at the 73% significance level) and significantly higher than undefined days (though not significantly
higher than non-event days). This means that on the days most likely to have regional new-particle
formation and growth at Egbert, the condensation sink is higher compared to other days. A higher
condensation sink must be offset by a higher production rate of low-volatility condensable material
425 (e.g. H₂SO₄ and low-volatility organics) to create favorable conditions for new-particle formation and
growth. As we discuss in the next subsection, the high condensation-sink days generally occurs when
air arrives from the heavily populated region to the south of Egbert.

The concentrations of SO₂, the precursor to condensable H₂SO₄ vapor, are highest on average on
class I event days followed by class II, undefined and non-event days. Class I days are not significantly
430 higher (only 88.6% significant) than class II days, but they are significantly higher than undefined and
non-event days. Undefined event days however, have 5 high-concentration outliers that exceed all of
the class I and II measurements. These class-2-event results may be indicative of plume-scale
new-particle formation in a coal-fired power-plant some other sulfur-rich plume (Junkermann et al.,
2011; Lonsdale et al., 2012; Stevens et al., 2012; Yu, 2010). In the next subsection, we will show that
435 the higher SO₂ days generally occur when air arrives from the heavily populated region to the south of
Egbert, similar to the condensation sink.

Finally, we use a proxy for H₂SO₄ concentration (Petäjä et al., 2009; Rohrer and Berresheim,
2006; Weber et al., 1997) to determine if H₂SO₄ concentrations are higher during regional new-particle
formation events than during other days. The proxy we use is:

$$440 \quad [H_2SO_4] \propto \frac{SR \cdot [SO_2]}{CS} \quad (2)$$

Where *SR* is the solar radiation and *CS* is the condensation sink. Note, this proxy is plotted on a log
scale. Although the condensation sink is highest on average for class I events, the H₂SO₄ proxy is
highest on average for class I days because both *SR* and SO₂ are highest on average for these days. The
distribution of the H₂SO₄ proxy on the I days is significantly different at the 95% level from class II
445 days (partly because of the higher mean and median, and partly because of the broader distribution).
Class I days are statistically different from undefined and non-event days, with higher means and
medians.

Unfortunately, we do not have measurements of organics throughout the time period used here, so we are limited to information on sulfuric acid. However, emissions of biogenic volatile organic compounds (precursors for secondary organics that may contribute to new-particle formation and growth (Riipinen et al., 2011, 2012)) are more favorable under warmer and sunnier conditions at Egbert (Leaitch et al., 2011) and elsewhere (Paasonen et al., 2013) and thus lead to organic aerosol formation under these conditions. Because class I events experience the highest amount of solar radiation and temperature anomalies on average, condensation of low-volatility organic vapors to a growing nucleation mode may be more favorable on these days.

While Figure 4 shows the distributions of environmental factors during events in the various classes, it does not show how new-particle-formation rates (J10) or growth rates (GR) vary with the values of these factors. Table 2 shows the correlation coefficients of J10 and GR with the 7 environmental factors in Figure 4 on class I days. Because J10s and GRs span several orders of magnitude we take the log of these quantities as well as the log of condensation sink, SO₂ and the H₂SO₄ proxy, which each span orders of magnitude (additionally, a log dependence of J with H₂SO₄ is consistent with the nucleation theorem). All of the environmental factors show stronger correlations (or anti-correlations) with J10 than with the GRs. This could be because other, independent factors (e.g. the condensation of low-volatility organics) are more important to GRs than to J10s. As would be expected, J10 is positively correlated with solar radiation, SO₂ and the H₂SO₄ proxy (albeit weakly). Oddly, J10 is also positively correlated with the condensation sink. However, the condensation sink is also positively correlated with SO₂ (correlation coefficient = 0.74, not shown), which offsets the dampening effect of condensation sink and leads to the weak positive correlation with the H₂SO₄ proxy. Because the correlation of the H₂SO₄ proxy with J10 is weak, it is likely that other species (e.g. organics) are contributing to J10s also.

3.3. Large-scale meteorology and back trajectories

In this section, we look at the regional meteorological features associated with the different types of events. Figure 5 shows the surface pressure anomaly (differences from the 4-week running mean centered on the event day) for the mean of class I, II and undefined event days (non-event days show only small deviations from the mean, so we have not plotted non-event days here). Regions with a statistically significant (95% confidence relative to randomly chosen sets of days) high surface pressure anomaly are shaded in pink, and regions where there is a statistically significant (95% confidence) low

surface pressure anomaly are shaded in blue. Statistical significance is computed following the bootstrap method (Efron, 1979; see Appendix A for details). Consistent with the high surface-pressure anomalies on class I event days measured at Egbert in Figure 4c, the entire region around Egbert exhibits a significant surface pressure anomaly of more than 300 Pa. Although not shown in Figure 5, Egbert is located inside a region with a 99.8% significant high anomaly. We note that not all of the 44 class I events exhibit anomalous high pressure over Egbert. 25% of the class I event days experienced low pressure anomalies at the site (Figure 4d). Class II events also exhibit a positive surface pressure anomaly (150 hPa) but this pattern is not statistically different from background variations. For undefined events, the composite meteorological surface pressure pattern is markedly different from that of class I and II events (Figure 5c). For undefined events, the region of higher surface pressure is located northeast of Egbert, with a region of low surface pressure to the southwest.

Figure 6 shows composites of the full 500-hPa geopotential height field (i.e. the anomalies have been added back to the mean). Similar to Figure 5, non-event days show only small deviations from the mean, so we have not plotted non-event days in Figure 6. The pink and blue areas show the regions of the statistically significant anomalies. There is a statistically significant geopotential height anomaly on class I days west of Egbert, placing Egbert to the east of the ridge. The east sides of the 500-hPa geopotential ridges are associated with tropospheric subsidence and surface highs, consistent with Figure 5. There are no significant height anomalies in the vicinity of Egbert for the class II or undefined days.

We also investigated the large-scale vertical velocity (ω) fields from NCEP (not shown), and consistent with the large-scale dynamics shown in Figures 5 and 6, found statistically significant subsidence over and around Egbert for the class I days. Class II days also showed subsidence over Egbert, but this pattern not statistically significant. Undefined days showed no major vertical-wind structure.

The NCEP diagnostics shown here suggest that the regional-scale new-particle formation events (class I) are often associated with the large-scale synoptic pattern with surface highs, large-scale subsidence and a ridge to the west and a trough to the east of Egbert. This is not entirely surprising since these conditions generally bring sunny conditions over the region of subsidence and allow for a homogeneous boundary layer (assuming somewhat spatially homogeneous emissions). These large-scale conditions may explain the measured solar radiation, relative humidity, temperature

anomaly and pressure anomaly presented in Figure 4; however, it is not clear if these conditions also drive the surface-wind directions associated with the high condensation sink and SO₂ concentration
510 seen in class I days in Figure 4. To explore this, we use HYPLIT back trajectories.

Figure 7 shows one 24-hour HYSPLIT back trajectory for each new-particle formation event from the three event classes (non-events are lumped with undefined events here as their trajectory distributions were similar). The trajectory from each event ends at the hour closest to the middle of the new-particle formation event (for non-event days, we take the 13:00, the mean middle of I events). The
515 trajectories are colored by the condensation sink during the new-particle formation event. Air masses for class I events are roughly equally likely to have spent time over regions to the north and south, and they are less likely to have come from the west or east. Class II, undefined events and non events are roughly equally likely to have spent time over regions to the north, west and south, and somewhat less likely to come from the east. However, for all event classes, higher condensation-sink air generally
520 came from the densely populated regions from the south with lower condensation-sink air generally from the north. Each event class exhibits cases with both lower and higher condensation-sink air. A similar analysis looking at SO₂ concentrations rather than condensation sink (not shown), showed a very similar pattern where high-SO₂ air came from the south and low-SO₂ air from the north. Thus, air from the south has both high SO₂ and high condensation sink on new-particle formation days for all
525 event classes, which is consistent with earlier studies at Egbert that found that polluted air most often is from the south (Rupakheti et al., 2005). These results are consistent with the correlation coefficient between SO₂ and condensation sink of 0.74 on class I days discussed earlier. Interestingly, the regional-scale new-particle formation events (class I and maybe class II) are roughly equally likely to occur in clean versus polluted air, which may have been due to the opposing effects of SO₂ and the
530 condensation sink on new-particle formation.

Figure 8 shows the same back trajectories but color coded by the pressure anomaly. The figure shows that for class I and class II days, the high pressure-anomaly days are generally associated with air flowing to Egbert from the north. A similar analysis looking at the solar radiation rather than the pressure anomaly (not shown) showed that high solar radiation days are also associated with air flow
535 from the north. Thus, the days with high pressure and solar radiation are generally different from the high SO₂ and condensation-sink (although there is some overlap between high pollution and high solar radiation on days coming from the southeast on class I days).

Taking into account all of the analyses in sections 3.2 and 3.3, it appears that regional-scale new-particle formation (class I and possibly class II events) at Egbert occurs under two different sets of conditions (1) days with the large-scale synoptic meteorology shown in Figures 5 and 6 with high surface pressure, large-scale subsidence and clear skies generally driving airflow from the clean regions, and (2) days with polluted (yet relatively homogeneously mixed) air flow from the south. For some cases when air comes from the southeast, both of these conditions are satisfied and the air is both polluted and exhibits favorable synoptic conditions. These two conditions for new-particle formation in the region near Egbert was also noted in Jeong et al. 2010), where they looked at new-particle formation at Egbert and three other sites in Southern Ontario for three weeks during the summer of 2007. As shown in Table 2, we find that J10 and growth rates are correlated with SO₂ and CS, which suggests that the regional new-particle events occurring in the polluted events from the south are generally more intense than the events occurring in the cleaner air from the north.

550 **4. Summary and conclusions**

In this paper, we use one year of aerosol size measurements at Egbert, ON, Canada from May 2007 through May 2008 to explore new-particle formation and growth to climate-relevant particle sizes at this site. We present both the statistics of formation rates, growth rates and survival probabilities as well as an analysis of the factors that may have contributed to the new-particle formation and growth. We find that the regional-scale new-particle formation event frequency peaks in the spring and fall (30-50% of the days) with minima in the winter and summer. The winter minimum may be due to a lack of biogenic organic precursors to new-particle formation and growth and lower solar radiation while the summer minimum may be due to lower SO₂ mixing ratios than the other seasons.

Observed new-particle formation rates range from less than 0.1 to close to 10 cm⁻³ s⁻¹ during the events (and are about 5-10 times lower when averaged over the event day). The 24-hour mean and median values, 0.13 and 0.12 cm⁻³ s⁻¹, are within the range of values found at 5 sites investigated by Westervelt et al. (2013). Growth rates range from less than 0.5 to over 10 nm hr⁻¹ with mean and median values of 3.1 and 2.0 nm hr⁻¹, also within the range of Westervelt et al. (2013).

We estimate that the mean formation rates of 50 and 100 nm particles on regional new-particle formation days are 0.039 and 0.022 cm⁻³ s⁻¹ (averaged over the full day). From this, we estimate that

regional new-particle formation events contribute about half of the climate-relevant particles; however, there is significant uncertainty in our calculation due to uncertainties in aerosol lifetime and changes in the boundary-layer height.

570 We find that regional new-particle formation events often occur under synoptic conditions associated with high surface pressure and large-scale subsidence that cause sunny conditions and clean-air flow from the north and west. However, new-particle formation also occurs when air flows from the polluted regions to the south and southwest of Egbert. This air is associated with high SO₂ concentrations and high aerosol condensation sinks. The new-particle formation rates tend to be faster during events under these south/southwest flow conditions.

575 A major factor missing from this analysis is the formation rates of secondary organic aerosol (SOA). SOA may form from biogenic volatile organic compounds emitted by vegetation in the region around Egbert or through anthropogenic volatile organic compounds emitted from industry to the south of Egbert. SOA has been shown to be a contributor to both particle formation and growth (Donahue et al., 2011; Metzger et al., 2010; Pierce et al., 2011; Riipinen et al., 2011), and thus variability in SOA
580 formation rates likely contribute to some of the variability in new-particle formation occurrence, new-particle formation rates, growth rates and survival probabilities reported here. However, we do not have measurements of aerosol composition or of SOA precursor gases for most of the time period explored in this paper and thus do not include it here.

This work provides statistical constraints for testing model predictions of new-particle
585 formation and growth rates (and the driving factors for these rates) at Egbert. Future work will involve comparing the statistics of new-particle formation, growth rates and survival probabilities of an aerosol microphysics model to the measured statistics shown here (similar to what was done in Westervelt et al. (2013)). Additionally, these data may be used to test if the meteorological and background chemical factors (e.g. SO₂) are similar between the simulations and measurements. These comparisons will
590 allow a comprehensive test of modeled new-particle formation and condensational growth schemes.

5. Appendix A: Statistical significance of meteorological patterns

The statistical significance of the meteorological patterns in Figures 5 and 6 are computed using

the Bootstrap method (Efron, 1979) to determine if regional-scale new-particle formation events (class I events and possibly class II events) were associated with distinct regional meteorology. We
595 summarize the bootstrap method here. We create 10,000 sets of 44 randomly sampled days (the number of class I days; 57 days for class II events and 164 for undefined events) of surface pressure anomalies, 500-hPa height anomalies and vertical wind anomalies from the NCEP database (from between 1997 and 2009) over the region shown in Figures 5 and 6. Like in Figures 4c and 4d, the anomalies are defined as differences from the 4-week running mean centered on the event day. We calculate the mean
600 anomalies at each grid point for each of the 10,000 sets. Then, at each location, if the observed anomaly falls outside of the 2.5th-97.5th percentile range (confidence interval) of the 10,000 sample-set, we say that the observed anomaly is statistically significant at 95% confidence using a two-tailed test.

6. Acknowledgements

We acknowledge the two anonymous reviewers for their comments that have improved this paper.
605 Funding was provided through Environment Canada's Grants and Contribution program (G&C 1300358).

7. References

- 610 Boy, M., Kulmala, M., Ruuskanen, T. M., Pihlatie, M., Reissell, A., Aalto, P. P., Keronen, P., Dal Maso, M., Hellen, H., Hakola, H., Jansson, R., Hanke, M. and Arnold, F.: Sulphuric acid closure and contribution to nucleation mode particle growth, *Atmos. Chem. Phys.*, 5, 863–878, 2005.
- Charlson, R. J., Schwartz, S. E., Hales, J. M., Cess, R. D., Coakley, J. A., Hansen, J. E. and Hofman, D. J.: Climate Forcing by Anthropogenic Aerosols, *Science* (80-.), 255(January 24), 423–430, 1992.
- 615 Crippa, P. and Pryor, S. C.: Spatial and temporal scales of new particle formation events in eastern North America, *Atmos. Environ.*, 75, 257–264 [online] Available from: <http://www.sciencedirect.com/science/article/pii/S1352231013003051> (Accessed 14 November 2013), 2013.
- Croft, B., Pierce, J. R. and Martin, R. V.: Interpreting Aerosol Lifetimes Using the GEOS-Chem Radionuclide Model, *Submitt. to Atmos. Chem. Phys.*, 2013.
- 620 Dal Maso, M., Kulmala, M., Dal Maso, M., Riipinen, I., Wagner, R., Hussein, T., Aalto, P. and

- Lehtinen, K. E. J.: Formation and growth of fresh atmospheric aerosols: eight years of aerosol size distribution data from SMEAR II, Hyytiälä, Finland, *Boreal Environ. Res.*, (October), 323–336 [online] Available from: http://repository.ju.edu.jo/Lists/English_Repository/Attachments/28542/ber10-323.pdf (Accessed 8 November 2013), 2005.
- 625 Donahue, N. M., Trump, E. R., Pierce, J. R. and Riipinen, I.: Theoretical constraints on pure vapor-pressure driven condensation of organics to ultrafine particles, *Geophys. Res. Lett.*, 38(16), L16801, doi:10.1029/2011GL048115, 2011.
- Draxler, R. .: HYSPLIT4 user's guide. NOAA Tech. Memo. ERL ARL-230, Silver Spring, MD., 1999.
- 630 Draxler, R. R. and Hess, G. D.: Description of the HYSPLIT_4 modeling system, NOAA Tech. Memo. ERL ARL-224, NOAA Air Resources Laboratory, Silver Spring, MD, Silver Spring, MD., 1997.
- Draxler, R. R. and Hess, G. D.: An overview of the HYSPLIT_4 modeling system of trajectories, dispersion, and deposition, *Australian Meteorol. Mag.*, 47, 295–308, 1998.
- 635 Dusek, U., Frank, G. P., Hildebrandt, L., Curtius, J., Schneider, J., Walter, S., Chand, D., Drewnick, F., Hings, S., Jung, D., Borrmann, S. and Andreae, M. O.: Size matters more than chemistry for cloud-nucleating ability of aerosol particles, *Science* (80-.), 312(5778), 1375–1378, 2006.
- Efron, B.: Bootstrap Methods: Another Look at the Jackknife, *Ann. Stat.*, 7(1), 1–26 [online] Available from: <http://projecteuclid.org/euclid.aos/1176344552> (Accessed 6 November 2013), 1979.
- 640 Ehn, M., Thornton, J. A, Kleist, E., Sipilä, M., Junninen, H., Pullinen, I., Springer, M., Rubach, F., Tillmann, R., Lee, B., Lopez-Hilfiker, F., Andres, S., Acir, I.-H., Rissanen, M., Jokinen, T., Schobesberger, S., Kangasluoma, J., Kontkanen, J., Nieminen, T., Kurtén, T., Nielsen, L. B., Jørgensen, S., Kjaergaard, H. G., Canagaratna, M., Maso, M. D., Berndt, T., Petäjä, T., Wahner, A., Kerminen, V.-M., Kulmala, M., Worsnop, D. R., Wildt, J. and Mentel, T. F.: A large source of low-volatility secondary organic aerosol., *Nature*, 506, 476–9, doi:10.1038/nature13032, 2014.
- 645 Forster, P., Ramaswamy, V., Artaxo, P., Berntsen, T., Betts, R., Fahey, D. W., Haywood, J., Lean, J., Lowe, D. C., Myhre, G., Nganga, J., Prinn, R., Raga, G., Schulz, M. and Dorland, R. V: Changes in atmospheric constituents and in radiative forcing, in *Climate change 2007: the physical science basis. contribution of working group I to the fourth assessment report of the intergovernmental panel on climate change*, edited by S. Solomon, D. Qin, M. Manning, Z. Chen, M. Marquis, K. B. Averyt, M. Tignor, and H. L. Miller, pp. 129–234, Cambridge University Press, Cambridge, United Kingdom and New York, NY, USA., 2007.
- 650 Hamed, A., Korhonen, H., Sihto, S.-L., Joutsensaari, J., Järvinen, H., Petäjä, T., Arnold, F., Nieminen, T., Kulmala, M., Smith, J. N., Lehtinen, K. E. J. and Laaksonen, A.: The role of relative humidity in continental new particle formation, *J. Geophys. Res.*, 116(D3), D03202, doi:10.1029/2010JD014186, 2011.
- 655 Jeong, C.-H., Evans, G. J., McGuire, M. L., Chang, R. Y.-W., Abbatt, J. P. D., Zeromskiene, K., Mozurkewich, M., Li, S.-M. and Leaitch, W. R.: Particle formation and growth at five rural and urban sites, *Atmos. Chem. Phys.*, 10(16), 7979–7995, doi:10.5194/acp-10-7979-2010, 2010.
- 660 Junkermann, W., Vogel, B. and Sutton, M. a.: The climate penalty for clean fossil fuel combustion, *Atmos. Chem. Phys.*, 11(24), 12917–12924, doi:10.5194/acp-11-12917-2011, 2011.
- Kalnay, E., Kanamitsu, M., Kistler, R., Collins, W., Deaven, D., Gandin, L., Iredell, M., Saha, S., White, G., Woollen, J., Zhu, Y., Leetmaa, A., Reynolds, R., Chelliah, M., Ebisuzaki, W., Higgins, W.,

- 665 Janowiak, J., Mo, K. C., Ropelewski, C., Wang, J., Jenne, R. and Joseph, D.: The NCEP/NCAR 40-Year Reanalysis Project, *Bull. Am. Meteorol. Soc.*, 77(3), 437–471, doi:10.1175/1520-0477(1996)077<0437:TNYRP>2.0.CO;2, 1996.
- 670 Kerminen, V.-M., Paramonov, M., Anttila, T., Riipinen, I., Fountoukis, C., Korhonen, H., Asmi, E., Laakso, L., Lihavainen, H., Swietlicki, E., Svenningsson, B., Asmi, A., Pandis, S. N., Kulmala, M. and Petäjä, T.: Cloud condensation nuclei production associated with atmospheric nucleation: a synthesis based on existing literature and new results, *Atmos. Chem. Phys.*, 12(24), 12037–12059, doi:10.5194/acp-12-12037-2012, 2012.
- Kuang, C., Chen, M., Zhao, J., Smith, J., McMurry, P. H. and Wang, J.: Size and time-resolved growth rate measurements of 1 to 5 nm freshly formed atmospheric nuclei, *Atmos. Chem. Phys.*, 12(7), 3573–3589, doi:10.5194/acp-12-3573-2012, 2012.
- 675 Kuang, C., McMurry, P. H. and McCormick, A. V.: Determination of cloud condensation nuclei production from measured new particle formation events, *Geophys. Res. Lett.*, 36(9), n/a–n/a, doi:10.1029/2009GL037584, 2009.
- Kulmala, M., Petaja, T., Monkkonen, P., Koponen, I. K., Dal Maso, M., Aalto, P. P., Lehtinen, K. E. J. and Kerminen, V. M.: On the growth of nucleation mode particles: source rates of condensable vapor in polluted and clean environments, *Atmos. Chem. Phys.*, 5, 409–416, 2005.
- 680 Kulmala, M., Petäjä, T., Nieminen, T., Sipilä, M., Manninen, H. E., Lehtipalo, K., Dal Maso, M., Aalto, P. P., Junninen, H., Paasonen, P., Riipinen, I., Lehtinen, K. E. J., Laaksonen, A. and Kerminen, V.-M.: Measurement of the nucleation of atmospheric aerosol particles., *Nat. Protoc.*, 7(9), 1651–67, doi:10.1038/nprot.2012.091, 2012.
- 685 Kulmala, M., Vehkamäki, H., Petaja, T., Dal Maso, M., Lauri, A., Kerminen, V. M., Birmili, W. and McMurry, P. H.: Formation and growth rates of ultrafine atmospheric particles: a review of observations, *J. Aerosol Sci.*, 35(2), 143–176, 2004.
- 690 Leaitch, W. R., Macdonald, A. M., Brickell, P. C., Liggio, J., Sjostedt, S. J., Vlasenko, A., Bottenheim, J. W., Huang, L., Li, S.-M., Liu, P. S. K., Toom-Saunty, D., Hayden, K. A., Sharma, S., Shantz, N. C., Wiebe, H. A., Zhang, W., Abbatt, J. P. D., Slowik, J. G., Chang, R. Y.-W., Russell, L. M., Schwartz, R. E., Takahama, S., Jayne, J. T. and Ng, N. L.: Temperature response of the submicron organic aerosol from temperate forests, *Atmos. Environ.*, 45(37), 6696–6704 [online] Available from: <http://www.sciencedirect.com/science/article/pii/S1352231011008843> (Accessed 10 October 2013), 2011.
- 695 Lonsdale, C. R., Stevens, R. G., Brock, C. a., Makar, P. a., Knipping, E. M. and Pierce, J. R.: The effect of coal-fired power-plant SO₂ and NO_x control technologies on aerosol nucleation in the source plumes, *Atmos. Chem. Phys.*, 12, 11519–11531, doi:10.5194/acpd-12-19683-2012, 2012.
- 700 Merikanto, J., Spracklen, D., Mann, G. W., Pickering, S. J. and Carslaw, K. S.: Impact of nucleation on global CCN, *Atmos. Chem. Phys.*, 9, 8601–8616 [online] Available from: <http://www.atmos-chem-phys-discuss.net/9/12999/2009/acpd-9-12999-2009.pdf> (Accessed 24 November 2012), 2009.
- Metzger, A., Verheggen, B., Dommen, J., Duplissy, J., Prevot, A. S. H., Weingartner, E., Riipinen, I., Kulmala, M., Spracklen, D. V, Carslaw, K. S. and Baltensperger, U.: Evidence for the role of organics in aerosol particle formation under atmospheric conditions., *Proc. Natl. Acad. Sci. U. S. A.*, 107(15), 6646–51, doi:10.1073/pnas.0911330107, 2010.

- 705 Paasonen, P., Asmi, A., Petäjä, T., Kajos, M. K., Äijälä, M., Junninen, H., Holst, T., Abbatt, J. P. D., Arneth, A., Birmili, W., van der Gon, H. D., Hamed, A., Hoffer, A., Laakso, L., Laaksonen, A., Richard Leaitch, W., Plass-Dülmer, C., Pryor, S. C., Räisänen, P., Swietlicki, E., Wiedensohler, A., Worsnop, D. R., Kerminen, V.-M. and Kulmala, M.: Warming-induced increase in aerosol number concentration likely to moderate climate change, *Nat. Geosci.*, 6(6), 438–442, doi:10.1038/ngeo1800, 2013.
- 710 Paramonov, M., Aalto, P. P., Asmi, A., Prisle, N., Kerminen, V.-M., Kulmala, M. and Petäjä, T.: The analysis of size-segregated cloud condensation nuclei counter (CCNC) data and its implications for cloud droplet activation, *Atmos. Chem. Phys.*, 13(20), 10285–10301, doi:10.5194/acp-13-10285-2013, 2013.
- 715 Petäjä, T., Mauldin III, R., Kosciuch, E., McGrath, J., Nieminen, T., Paasonen, P., Boy, M., Adamov, A., Kotiaho, T. and Kulmala, M.: Sulfuric acid and OH concentrations in a boreal forest site, *Atmos. Chem. Phys.*, 9, 7435–7448 [online] Available from: <http://www.atmos-chem-phys.net/9/7435/2009/> (Accessed 10 October 2013), 2009.
- Pierce, J. R. and Adams, P. J.: Efficiency of cloud condensation nuclei formation from ultrafine particles, *Atmos. Chem. Phys.*, 7, 1367–1379, 2007.
- 720 Pierce, J. R. and Adams, P. J.: Uncertainty in global CCN concentrations from uncertain aerosol nucleation and primary emission rates, *Atmos. Chem. Phys.*, 9(4), 1339–1356, doi:10.5194/acp-9-1339-2009, 2009.
- 725 Pierce, J. R., Leaitch, W. R., Liggio, J., Westervelt, D. M., Wainwright, C. D., Abbatt, J. P. D., Ahlm, L., Al-Basheer, W., Cziczo, D. J., Hayden, K. L., Lee, A. K. Y., Li, S.-M., Russell, L. M., Sjostedt, S. J., Strawbridge, K. B., Travis, M., Vlasenko, A., Wentzell, J. J. B., Wiebe, H. A., Wong, J. P. S. and Macdonald, A. M.: Nucleation and condensational growth to CCN sizes during a sustained pristine biogenic SOA event in a forested mountain valley, *Atmos. Chem. Phys.*, 12(7), 3147–3163, doi:10.5194/acp-12-3147-2012, 2012.
- 730 Pierce, J. R., Riipinen, I., Kulmala, M., Ehn, M., Petäjä, T., Junninen, H., Worsnop, D. R. and Donahue, N. M.: Quantification of the volatility of secondary organic compounds in ultrafine particles during nucleation events, *Atmos. Chem. Phys.*, 11(17), 9019–9036, doi:10.5194/acp-11-9019-2011, 2011.
- 735 Riipinen, I., Pierce, J. R., Yli-Juuti, T., Nieminen, T., Häkkinen, S., Ehn, M., Junninen, H., Lehtipalo, K., Petäjä, T., Slowik, J., Chang, R., Shantz, N. C., Abbatt, J., Leaitch, W. R., Kerminen, V.-M., Worsnop, D. R., Pandis, S. N., Donahue, N. M. and Kulmala, M.: Organic condensation: a vital link connecting aerosol formation to cloud condensation nuclei (CCN) concentrations, *Atmos. Chem. Phys.*, 11(8), 3865–3878, doi:10.5194/acp-11-3865-2011, 2011.
- Riipinen, I., Yli-Juuti, T., Pierce, J. R., Petäjä, T., Worsnop, D. R., Kulmala, M. and Donahue, N. M.: The contribution of organics to atmospheric nanoparticle growth, *Nat. Geosci.*, 5(7), 453–458, doi:10.1038/ngeo1499, 2012.
- 740 Rupakheti, M., Leaitch, W. R., Lohmann, U., Hayden, K., Brickell, P., Lu, G., Li, S.-M., Toom-Saunty, D., Bottenheim, J. W., Brook, J. R., Vet, R., Jayne, J. T. and Worsnop, D. R.: An Intensive Study of the Size and Composition of Submicron Atmospheric Aerosols at a Rural Site in Ontario, Canada, *Aerosol Sci. Technol.*, 39(8), 722–736, doi:10.1080/02786820500182420, 2005.
- 745 Seinfeld, J. H. and Pandis, S. N.: *Atmospheric Chemistry and Physics*, 1st ed., John Wiley and Sons., New York., 2006.
- Sihto, S.-L., Kulmala, M., Kerminen, V.-M., Dal Maso, M., Petaja, T., Riipinen, I., Korhonen, H.,

- Arnold, F., Janson, R., Boy, M., Laaksonen, A. and Lehtinen, K. E. J.: Atmospheric sulphuric acid and aerosol formation: implications from atmospheric measurements for nucleation and early growth mechanisms, *Atmos. Chem. Phys.*, 6, 4079–4091, 2006.
- 750 Slowik, J. G., Stroud, C., Bottenheim, J. W., Brickell, P. C., Chang, R. Y.-W., Liggio, J., Makar, P. A., Martin, R. V., Moran, M. D., Shantz, N. C., Sjostedt, S. J., van Donkelaar, A., Vlasenko, A., Wiebe, H. A., Xia, A. G., Zhang, J., Leaitch, W. R. and Abbatt, J. P. D.: Characterization of a large biogenic secondary organic aerosol event from eastern Canadian forests, *Atmos. Chem. Phys.*, 10(6), 2825–2845, doi:10.5194/acp-10-2825-2010, 2010.
- 755 Spracklen, D. V, Carslaw, K. S., Kulmala, M., Kerminen, V. M., Mann, G. W. and Sihto, S. L.: The contribution of boundary layer nucleation events to total particle concentrations on regional and global scales, *Atmos. Chem. Phys.*, 6, 5631–5648, 2006.
- 760 Stevens, R. G. and Pierce, J. R.: A parameterization of sub-grid particle formation in sulphur-rich plumes for global and regional-scale models, *Atmos. Chem. Phys. Discuss.*, 13(7), 19583–19623, doi:10.5194/acpd-13-19583-2013, 2013.
- Stevens, R. G., Pierce, J. R., Brock, C. A., Reed, M. K., Crawford, J. H., Holloway, J. S., Ryerson, T. B., Huey, L. G. and Nowak, J. B.: Nucleation and growth of sulfate aerosol in coal-fired power plant plumes: sensitivity to background aerosol and meteorology, *Atmos. Chem. Phys.*, 12(1), 189–206, doi:10.5194/acp-12-189-2012, 2012.
- 765 Vehkamäki, H., Kulmala, M., Napari, I., Lehtinen, K. E. J., Timmreck, C., Noppel, M. and Laaksonen, A.: An improved parameterization for sulfuric acid-water nucleation rates for tropospheric and stratospheric conditions, *J. Geophys. Res.*, 107(D22), 4610–4622, 2002.
- 770 Westervelt, D. M., Pierce, J. R., Riipinen, I., Trivittayanurak, W., Hamed, A., Kulmala, M., Laaksonen, A., Decesari, S. and Adams, P. J.: Formation and growth of nucleated particles into cloud condensation nuclei: model–measurement comparison, *Atmos. Chem. Phys.*, 13(15), 7645–7663, doi:10.5194/acp-13-7645-2013, 2013.
- Yu, F.: Diurnal and seasonal variations of ultrafine particle formation in anthropogenic SO₂ plumes., *Environ. Sci. Technol.*, 44(6), 2011–5, doi:10.1021/es903228a, 2010.

775

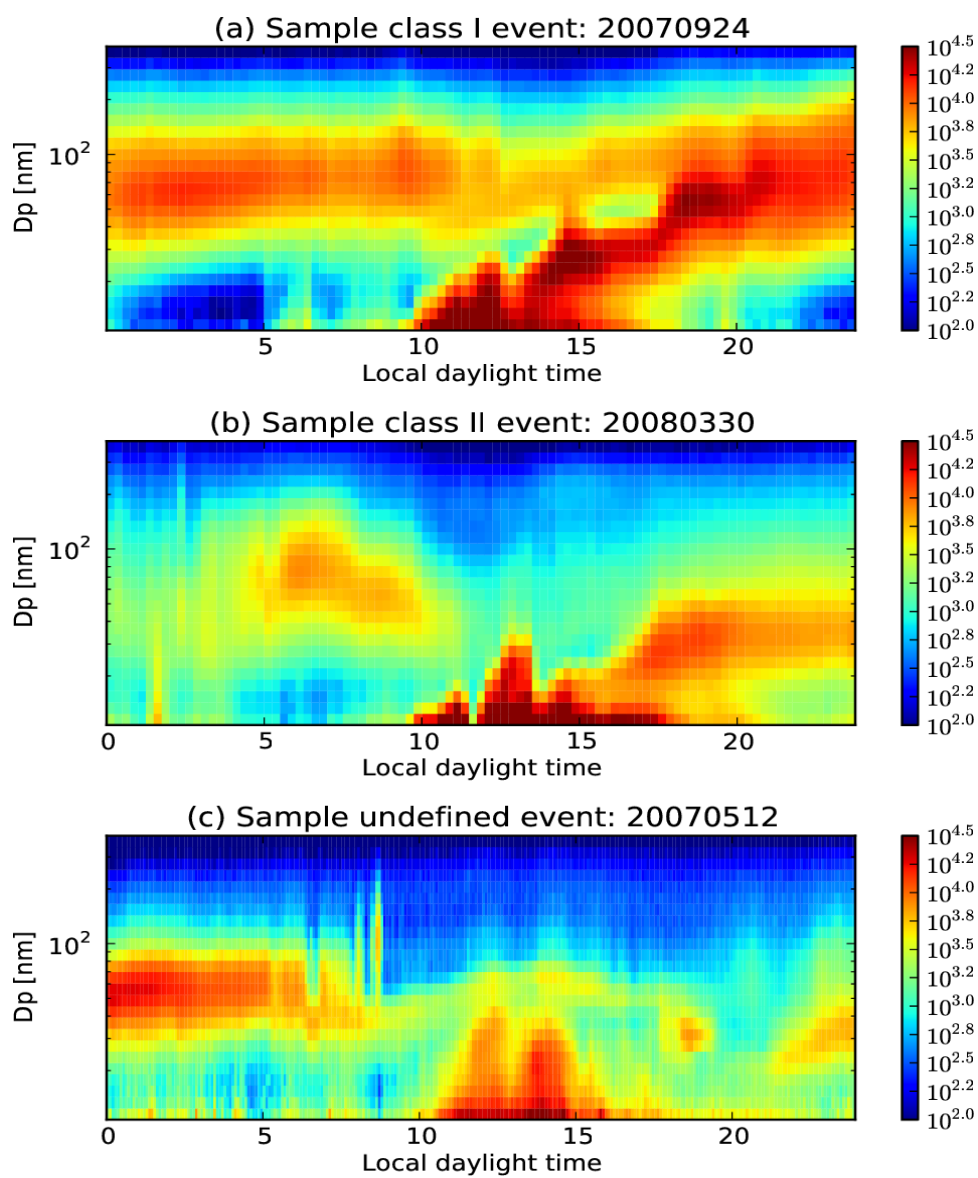
Table 1. Means and medians of nucleation, growth and CCN-formation parameters across all days of each event class.

Class	# of days	J10	J10 (24-hr)	GR	SP50	SP100	J50 (24-hr)	J100 (24-hr)
		cm ⁻³ s ⁻¹	cm ⁻³ s ⁻¹	nm hr ⁻¹	%	%	cm ⁻³ s ⁻¹	cm ⁻³ s ⁻¹
I (means)	44	0.84	0.13	3.1	33	19	0.039	0.022
I (medians)	44	0.64	0.12	2.4	19	7	0.029	0.0091
II (means)	57	0.58	0.069	3.1	N/A	N/A	N/A	N/A
II (medians)	57	0.22	0.049	2.0	N/A	N/A	N/A	N/A
I+II (means)	101	0.69	0.097	3.1	N/A	N/A	N/A	N/A
I+II (medians)	101	0.30	0.050	2.2	N/A	N/A	N/A	N/A

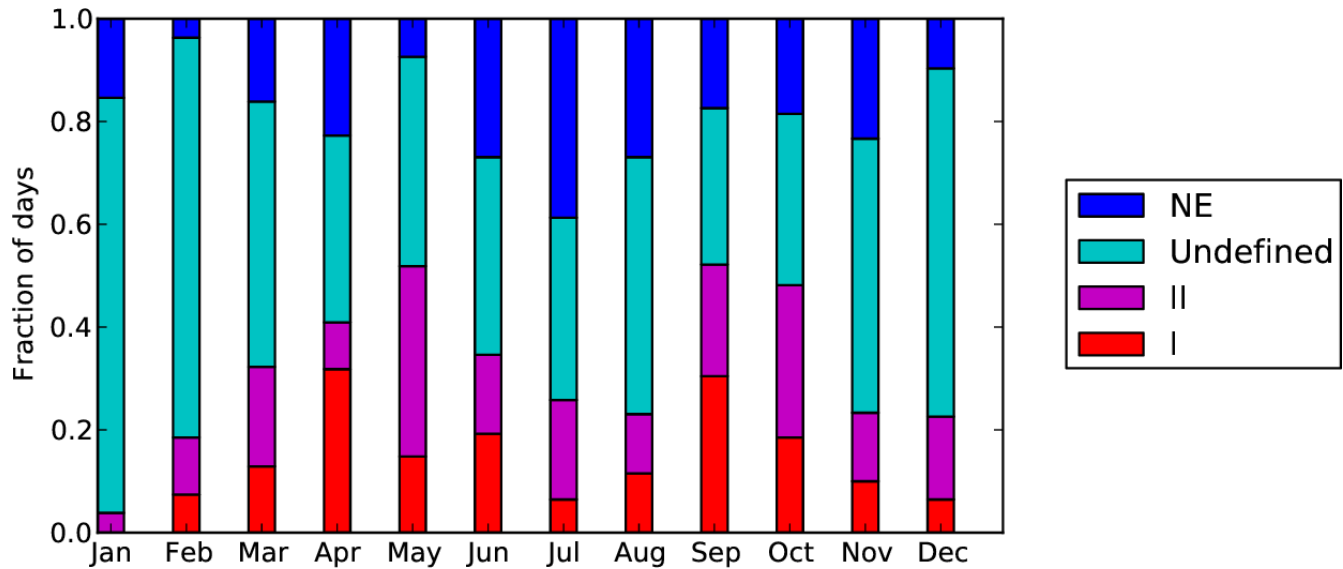
Table 2. Correlation coefficients between environmental factors with J10s and GRs on class I days.

	log(J10)	log(GR)
Solar radiation	0.42	0.06
RH	-0.26	0.10
T anomaly	0.27	0.16
P anomaly	-0.14	-0.03
log(Condensation sink)	0.44	0.18
log(SO ₂ mixing ratio)	0.33	0.23
log(SR·SO ₂ /CS)	0.20	0.12

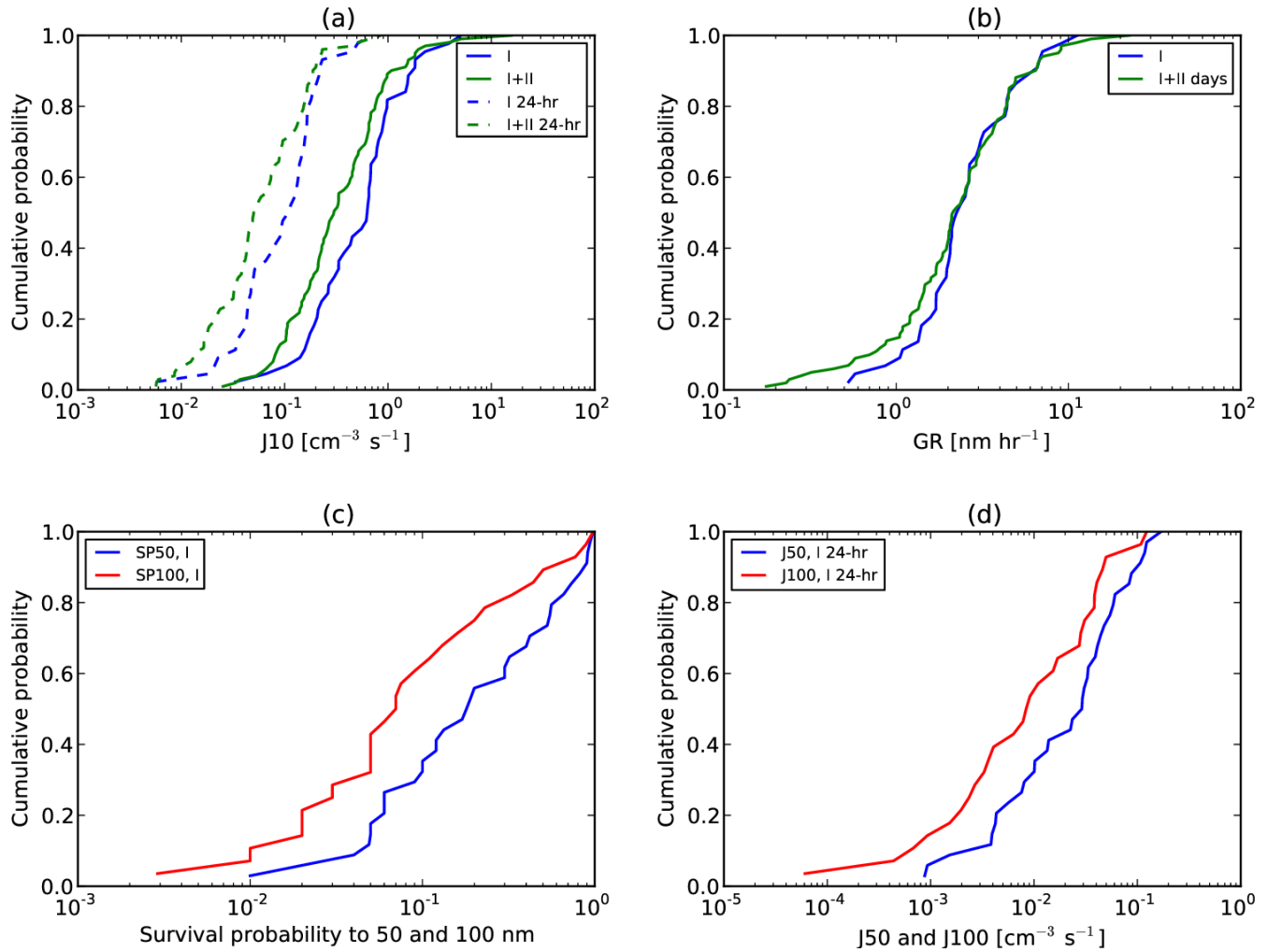
780



785 Figure 1. Sample size-distribution time series for a (a) class I nucleation day, (b) class II nucleation day and (c) undefined nucleation day. The color axis is $dN/d\log D_p$ [cm^{-3}].

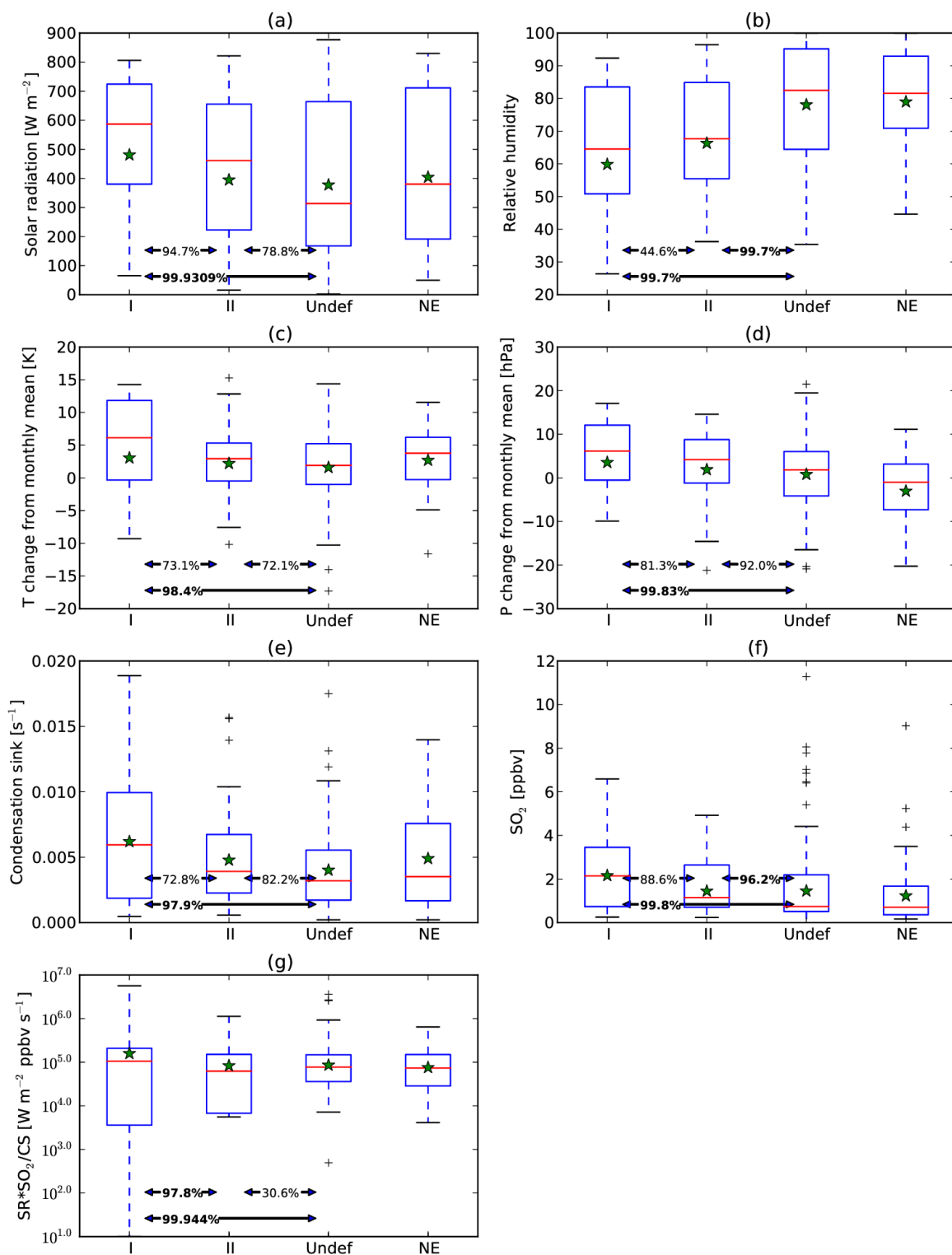


790 Figure 2. The fraction of days in each month classified as having class I, II and undefined events as well as days with no events (NE). Some days did not have at least 75% of the day with SMPS data and were not used. All months had at least 22 classified days. Note that multiple undefined events may occur on a given undefined event day. Undefined events may also occur on class I or class II event days; however, these are counted as I or II days.



800

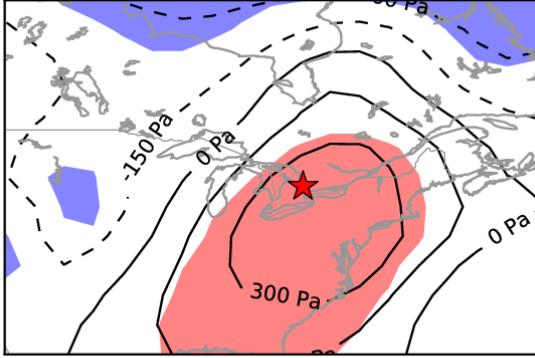
Figure 3: Cumulative probability distributions of various nucleation and growth metrics from the full year. Panel (a): J10 rates for both I days and I+II days. Solid lines show the rates averaged only over the period where nucleation was occurring. Dashed lines show the rates averaged over the full day. Panel (b): Growth rates for both I days and I+II days. For the following panels, only I days are shown as we do not trust the estimates of survival probability for II days. Panel (c): Survival probability to 50 and 100 nm. Panel (e): 24-hour-mean production rate of 50 and 100 nm particles.



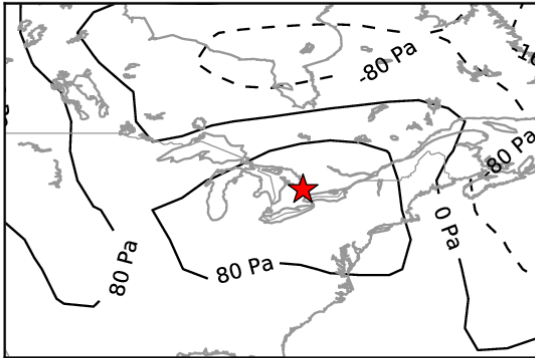
805 Figure 4. Box-whisker plots of various meteorological variables as well as the condensation sink, SO_2 mixing ratio and a H_2SO_4 proxy for class I, II, undefined and non-event days. The values are calculated between the start and end of new-particle formation on each day except for non-event days where the full day is used. The red line shows the median values. Stars show the mean values. The box shows the interquartile range (IQR, 25th and 75th percentile). The whiskers show the lowest datum still within 1.5 IQR of the lower quartile, and the highest datum still within 1.5 IQR of the upper quartile. Crosses

810 show data outside of 1.5 IQR above or below the upper or lower quartile. The percentages shown in
between each box show the probability that the distributions are statistically different (calculated using
the Mann–Whitney U test). Although not shown on the plots, the distributions for 1a days are
statistically different from non-event days to at least the 98% level for all factors except condensation
sink (89%). Panel (a) solar radiation, (b) relative humidity, (c) temperature change from the running
815 28-day mean (14 days before to 14 days after, to remove the season cycle), (d) surface pressure change
from the running 28-day mean, (e) condensation sink, (f) SO₂ mixing ratio, (g) H₂SO₄ proxy
(SR*SO₂/condensation_sink).

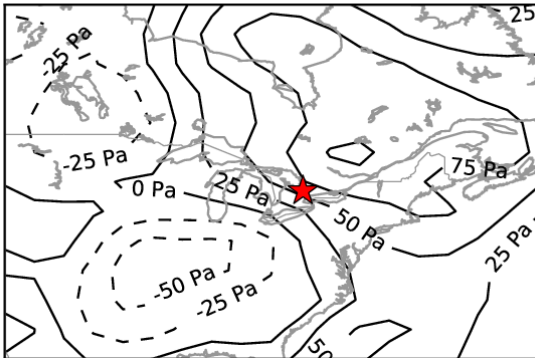
a) Class I days: Surface pressure anomaly [Pa]



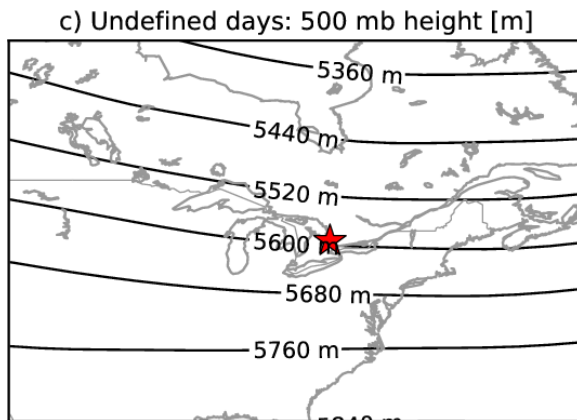
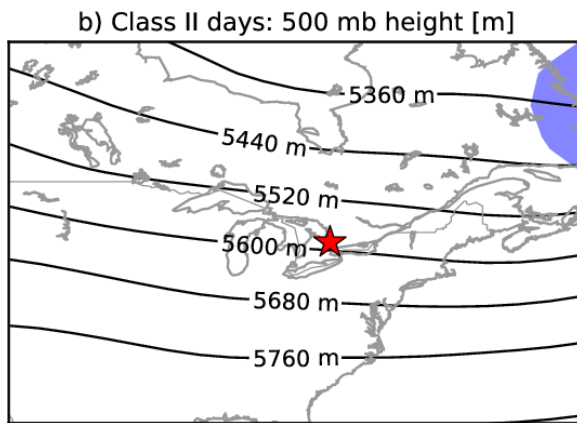
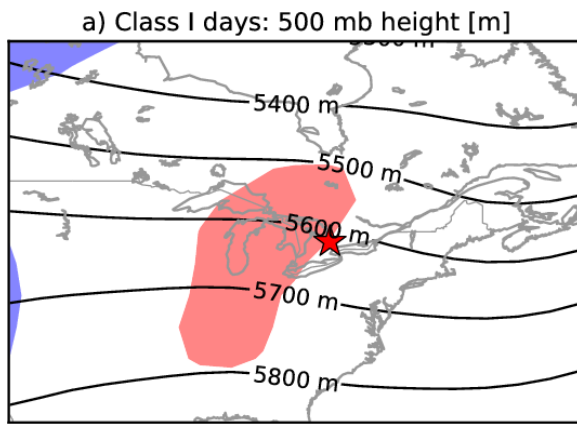
b) Class II days: Surface pressure anomaly [Pa]



c) Undefined days: Surface pressure anomaly [Pa]

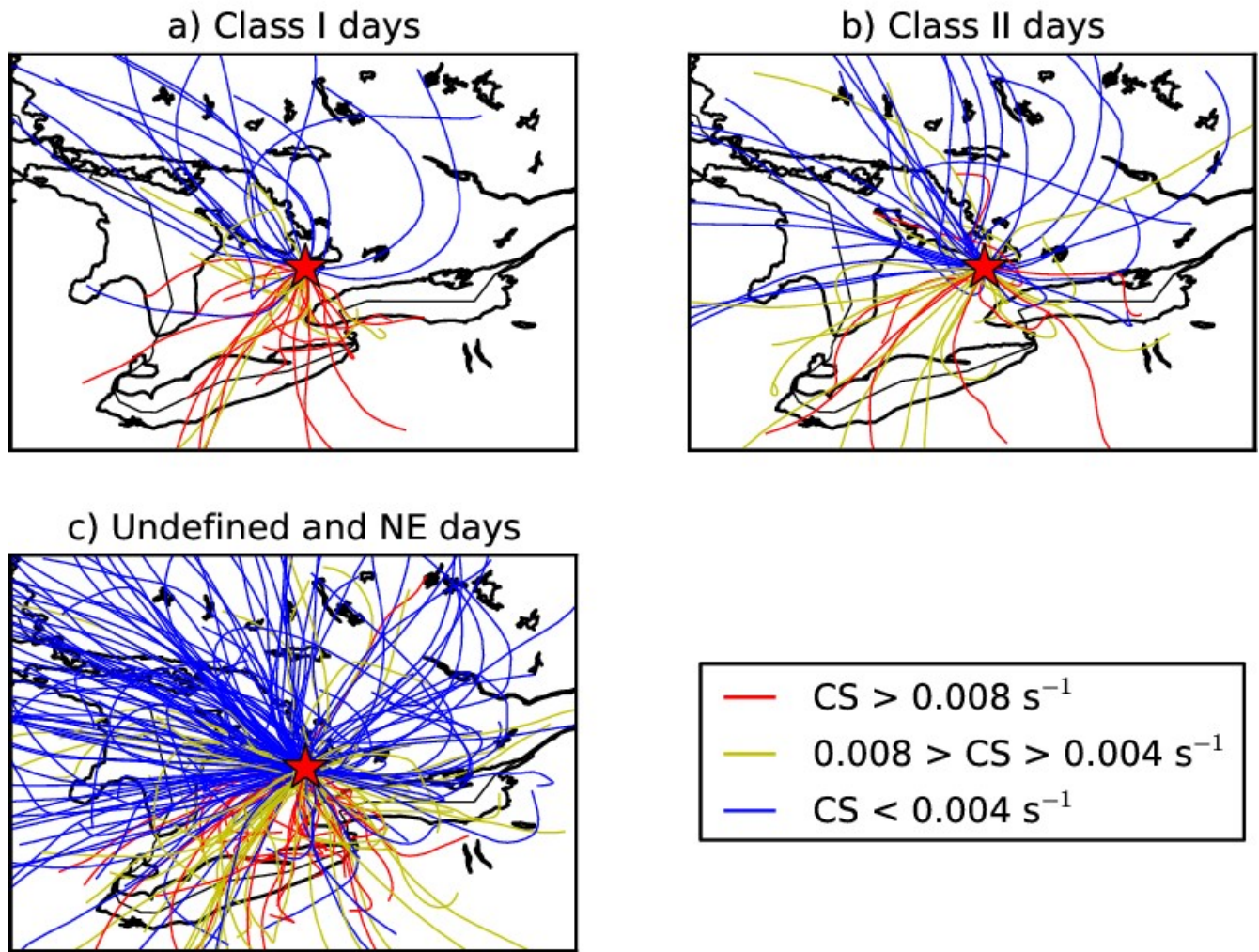


820 Figure 5. NCEP reanalysis surface pressure anomaly [Pa] from the 28-day mean for (a) class I days, (b) II days, and (c) undefined days. Positive 95% significance anomalies are shaded in pink and negative 95% significance anomalies are shaded in blue.



825 Figure 6. NCEP reanalysis mean 500 mb geopotential heights [m] for (a) class I days, (b) II days, and (c) undefined days. Positive 95% significance anomalies are shaded in pink and negative 95% significance anomalies are shaded in blue.

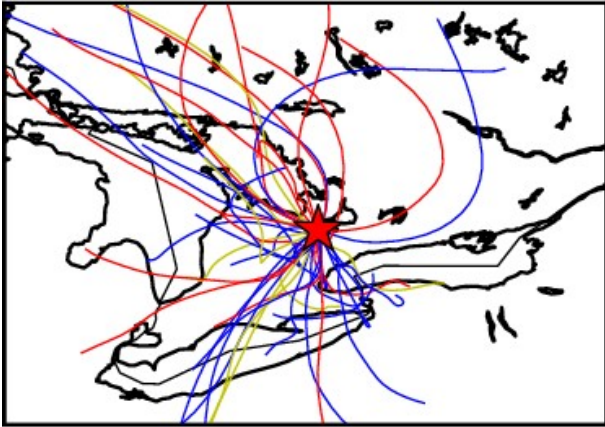
CS



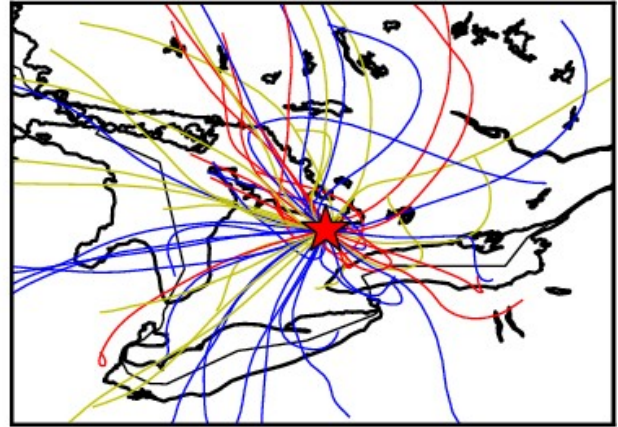
830 Figure 7. 24-hour back trajectories arriving during the new-particle formation event during each class I, II and undefined+non-event day (one back trajectory per event). Trajectories are color-coded by the condensation sink measured during the event.

P anomaly

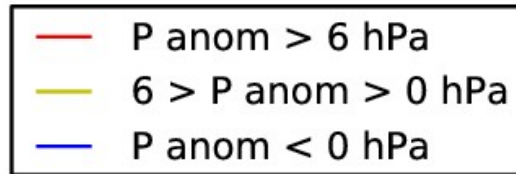
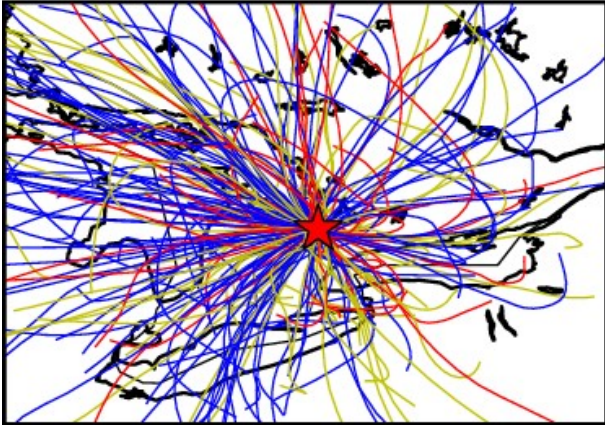
a) Class I days



b) Class II days



c) Undefined and NE days



835 Figure 8. 24-hour back trajectories arriving during the new-particle formation event during each class I, II and undefined+non-event day (one back trajectory per event). Trajectories are color-coded by the surface pressure anomaly (from the 28-day running mean) measured during the event.